Electronic Supplementary Material (ESI) for Photochemical & Photobiological Sciences.

Synthesis of Ag-Ho, Ag-Sm, Ag-Zn, Ag-Cu, Ag-Cs, Ag-Zr, Ag-Er, Ag-Y and Ag-Co metal organic nanoparticles for UV-Vis-NIR wide-range bio-tissue imaging

Ye Wu, Yingcheng Lin, and Jian Xu

Content

Section 1. Schematic of the NIR fluorescence spectra/imaging setup.

(a)

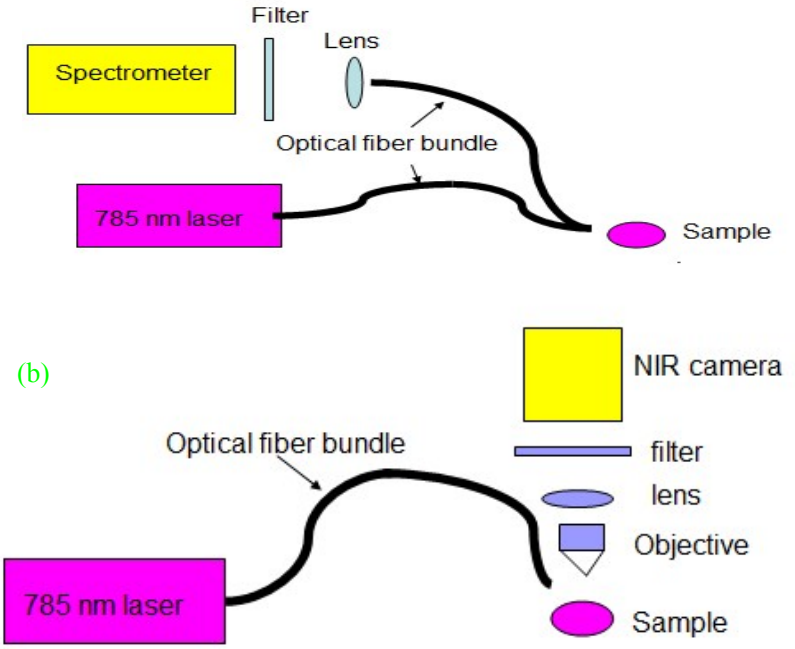

Figure S1. (a) Schematic of the NIR fluorescence spectra measurement setup. (b) Schematic of the NIR fluorescence imaging setup.

Section 2. Nanoparticle size, XRD spectra and Crystal structure information.

Name of compounds	Size(average)
Ag-Ho	6 nm
Ag-Sm	46.7 nm
Ag-Zn	93.9 nm
Ag-Cu	4.8 nm
Ag-Cs	49 nm
Ag-Zr	159.5 nm
Ag-Er	119 nm
Ag-Y	108 nm
Ag-Co	15 nm

Table S1. List of nanoparticles size for Ag-Ho, Ag-Sm, Ag-Zn, Ag-Cu, Ag-Cs, Ag-Zr, Ag-Er, Ag-Y and Ag-Co compounds.

The crystal structure of Ag-Ho, Ag-Sm, Ag-Zn, Ag-Cu, Ag-Cs, Ag-Zr, Ag-Er, Ag-Y and Ag-Co was solved by GSAS software package. The unit cells were drawn by DRAWxtl V5.5 package.

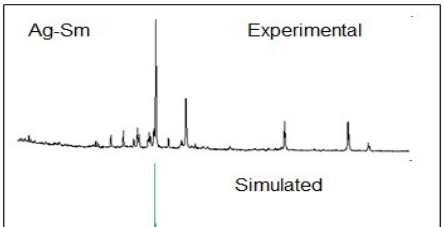

Figure S2. Simulated and experimental XRD profile of Ag-Sm compound.

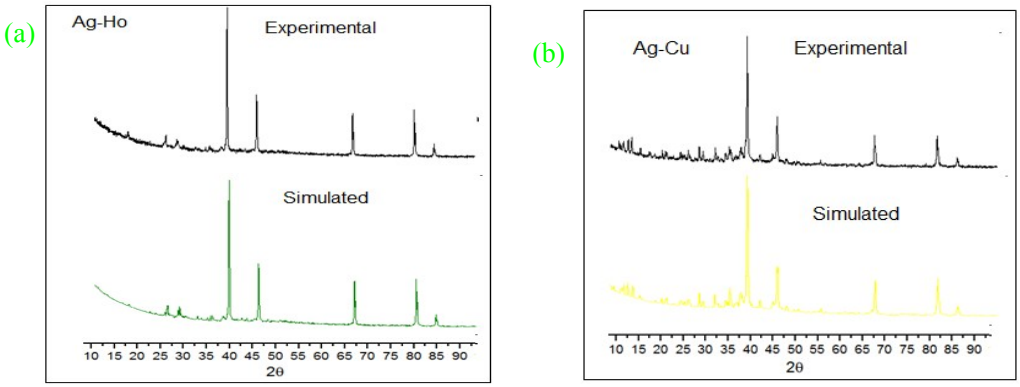

Figure S 3. (a) Simulated and experimental XRD profile of Ag-Ho compound. (b) Simulated and experimental XRD profile of Ag-Cu compound.

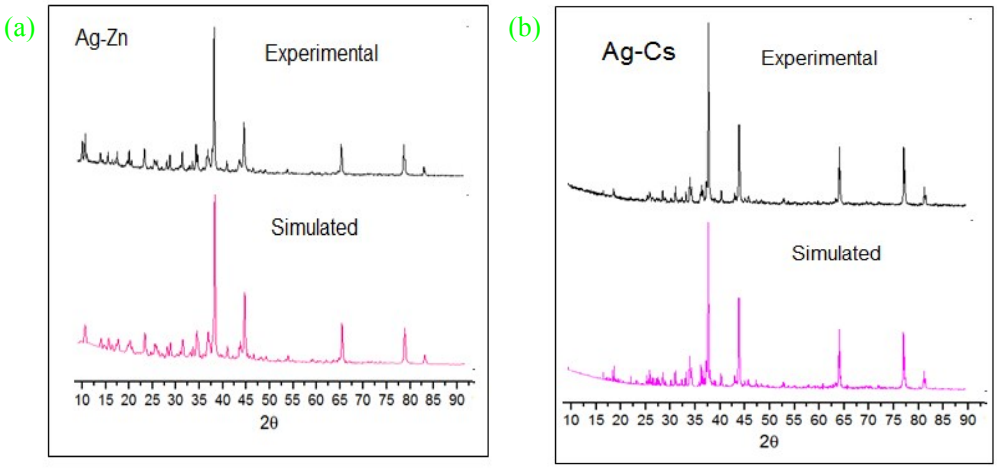

Figure S 4. (a) Simulated and experimental XRD profile of Ag-Zn compound. (b) Simulated and experimental XRD profile of Ag-Cs compound.

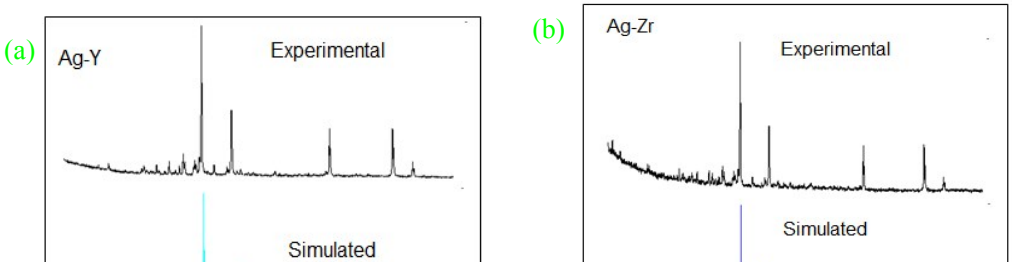

Figure S 5. (a) Simulated and experimental XRD profile of Ag-Y compound. (b) Simulated and experimental XRD profile of Ag-Zr compound.

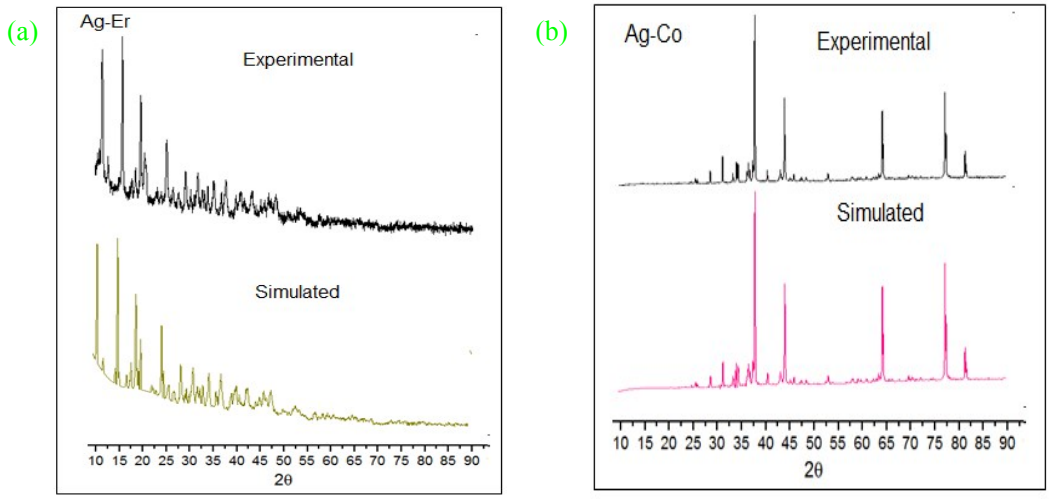

Figure S 6. (a) Simulated and experimental XRD profile of Ag-Er compound. (b) Simulated and experimental XRD profile of Ag-Co compound.

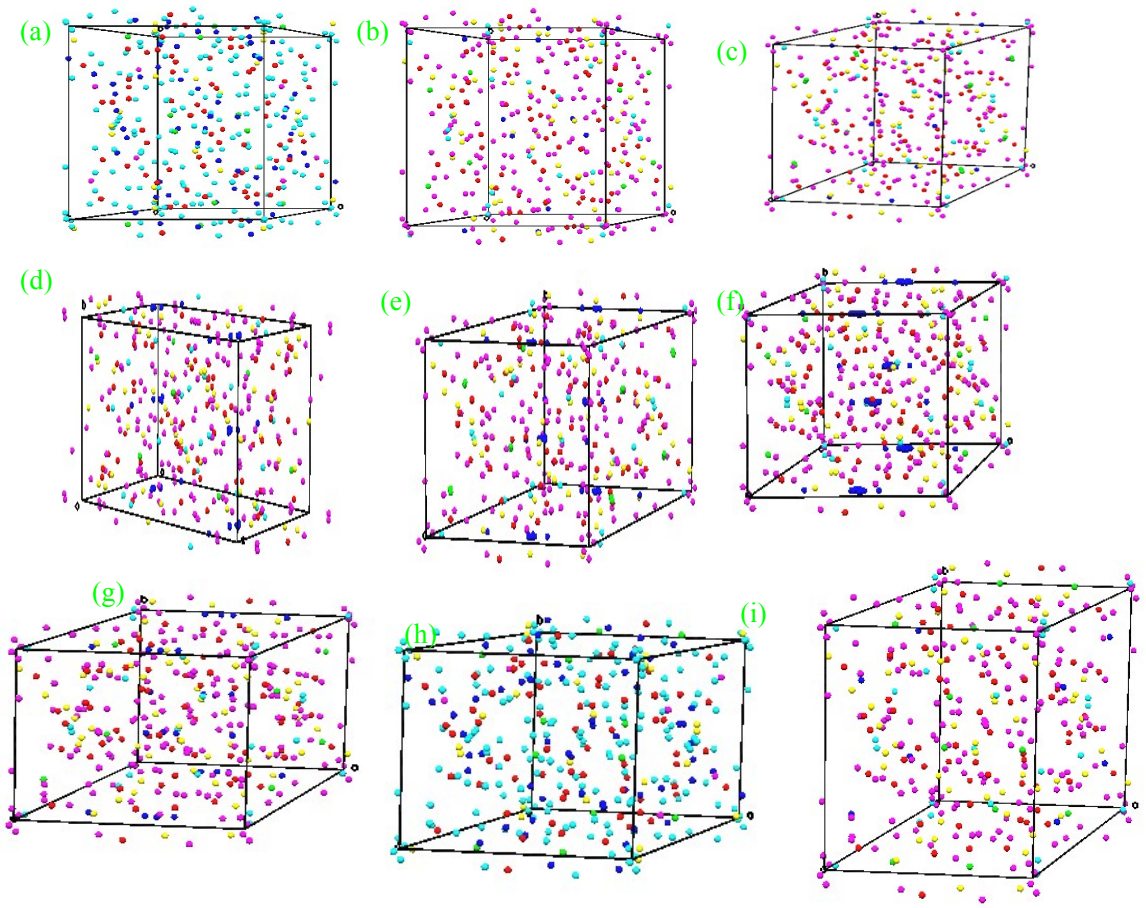

Figure S7. (a) Cell structure diagram of Ag-Ho compound (Red sphere: H; green sphere: Ag; Blue sphere: C; Yellow sphere: S; Cyan sphere: O; Magenta sphere: Ho). (b) Cell structure diagram of Ag-Zn compound.(Red sphere: H; Green sphere: Zn; Blue sphere: Ag; Yellow sphere: C; Cyan sphere: S; Magenta sphere: O). (c) Cell structure diagram of Ag-Cu compound (Red sphere: H; Green sphere: Cu; Blue sphere: Ag; Yellow sphere: C; Cyan sphere: S; Magenta sphere: O). (d)Cell structure diagram of Ag-Sm compound (Red sphere: H; Green sphere: Sm; Blue sphere: Ag; Yellow sphere: C; Cyan sphere: S; Magenta sphere: O). (e)Cell structure diagram of Ag-Y compound (Red sphere: H; Green sphere: Ag; Blue sphere: Y; Yellow sphere: C; Cyan sphere:S; Magenta sphere:O). (f)Cell structure diagram of Ag-Cs compound (Red sphere: H; Green sphere: Ag; Blue sphere: Cs; Yellow sphere: C; Cyan sphere: S; Magenta sphere: O). (g)Cell structure diagram of Ag-Zr compound (Red sphere: H; Green sphere: Zr; Blue sphere: Ag; Yellow sphere: C; Cyan sphere: S; Magenta sphere: O). (h) Cell structure diagram of Ag-Er compound(Red sphere: H; Green sphere: Ag; Blue sphere: C; Yellow sphere: S; Cyan sphere: O; Magenta sphere: Er).(i) Cell structure diagram of Ag-Co compound (Red sphere: H; Green sphere: Ag; Blue sphere: Co; Yellow sphere: C; Cyan sphere: S; Magenta sphere: O).

molecular formula	$C_6H_8Ag_2Ho\ O_{21}S_3$

cell length	a=12.190, b=14.202, c=17.454.
cell angle	α=90˚,β=107.195˚,γ=90˚
symmetry	monoclinic
space group	P 21/c

Table S2. Crystal information of Ag-Ho compound

molecular formula	$C_6H_8Ag_2O_{21}S_3Zn$
cell length	a=13.788, b=14.222, c=17.463
cell angle	α=90˚,β=107.288˚,γ=90˚
symmetry	monoclinic
space group	P 21/c

Table S3. Crystal information of Ag-Zn compound

molecular formula	$C_6H_8Ag_2Cu_2O_{21}S_3$
cell length	a=12.192, b=14.211, c=17.468
cell angle	α=90˚,β=107.235˚,γ=90˚
symmetry	monoclinic
space group	P 21/c

Table S4. Crystal information of Ag-Cu compound

molecular formula	$C_6H_8Ag_7O_{21}S_3Sm$
cell length	a=12.952, b=10.366, c=20.636
cell angle	α=90˚,β=103.283˚,γ=90˚
symmetry	monoclinic
space group	P 21/c

Table S5. Crystal information of Ag-Sm compound

molecular formula	$C_6H_8Ag\ Cs_{12}\ O_{21}S_3$
cell length	a=12.952, b=10.367, c=20.631.
cell angle	α=90˚,β=103.279˚,γ=90˚
symmetry	monoclinic
space group	P 21/c

Table S6. Crystal information of Ag-Cs compound

molecular formula	$C_6H_8Ag_4O_{21}S_3Zr$
cell length	a=12.952, b=10.366, c=20.623.
cell angle	α=90˚,β=103.299˚,γ=90˚
symmetry	monoclinic
space group	P 21/c

Table S7. Crystal information of Ag-Zr compound

molecular formula	$C_6H_8Ag_2O_{21}S_3Y_7$

cell length	a=12.949, b=10.364, c=20.619.
cell angle	α=90˚,β=103.286˚,γ=90˚
symmetry	monoclinic
space group	P 21/c

Table S8. Crystal information of Ag-Y compound

molecular formula	$C_6H_8Ag_2CoO_{21}S_3$
cell length	a=12.194, b=14.206, c=17.456
cell angle	α=90˚,β=107.18˚,γ=90˚
symmetry	monoclinic
space group	P 21/c

Table S9. Crystal information of Ag-Co compound

molecular formula	$C_6H_8Ag_2ErO_{21}S_3$
cell length	a=12.452, b=10.361, c=20.585.
cell angle	α=90˚,β=103.319˚,γ=90˚
symmetry	monoclinic
space group	P 21/c

Table S10. Crystal information of Ag-Er compound

Section 3. XPS analysis.

This section will show the detailed XPS analysis of Ag-Sm, Ag-Zn, Ag-Cu, Ag-Cs, Ag-Zr, Ag-Er, Ag-Y and Ag-Co (Note: the references for the following are listed at the end of Supportive Informaiton.)

For Ag-Zn compound(see Figure S8), the XPS spectra of Zn 2p show characteristic peaks at 1021 eV and 1044 eV, which are corresponding to Zn $2p_{3/2}$, Zn $2p_{1/2}$.[s1] The XPS spectra of Ag 3d present peaks at 367.3 eV and 373.3 eV, which are corresponding to core level of Ag $3d_{5/2}$ and Ag $3d_{3/2}$. Similar peaks can be found in Ag $3d_{5/2}$ and Ag $3d_{3/2}$ spectra of Ag_2O, which may suggest the forming of Ag-O bonding. [s2] Deconvolution of S 2p spectra shows peaks at 160.4 eV, 162.9 eV, 164.1 eV, 164.8 eV, 165.8 eV, 167.4 eV. They are attributed to S-O bonding.[s3] It should be mentioned that the peaks at 160.4 eV, 162.9 eV, 164.1eV are attributed to S $2p_{3/2}$ core level while the peak at 164.8 eV and 165.8 eV are considered as S $2p_{1/2}$ core level.[S3] The spectra of C 1s produces a major peak at 284.2 eV and two minor peak at 285.4 eV, 288.1 eV. The peak at 284.2 eV is assigned to C-C bonding, similar to that of graphite bulk.[s4] The peak at 285.4 eV is assigned to C-O-C bonding. The peak at 288.1 eV is assigned to O-C=O.[s5] O1s spectra produce peaks at 531.2eV and 532.6 eV, which are assigned to C-O bonding and C-O-H bonding, [s4,s6]

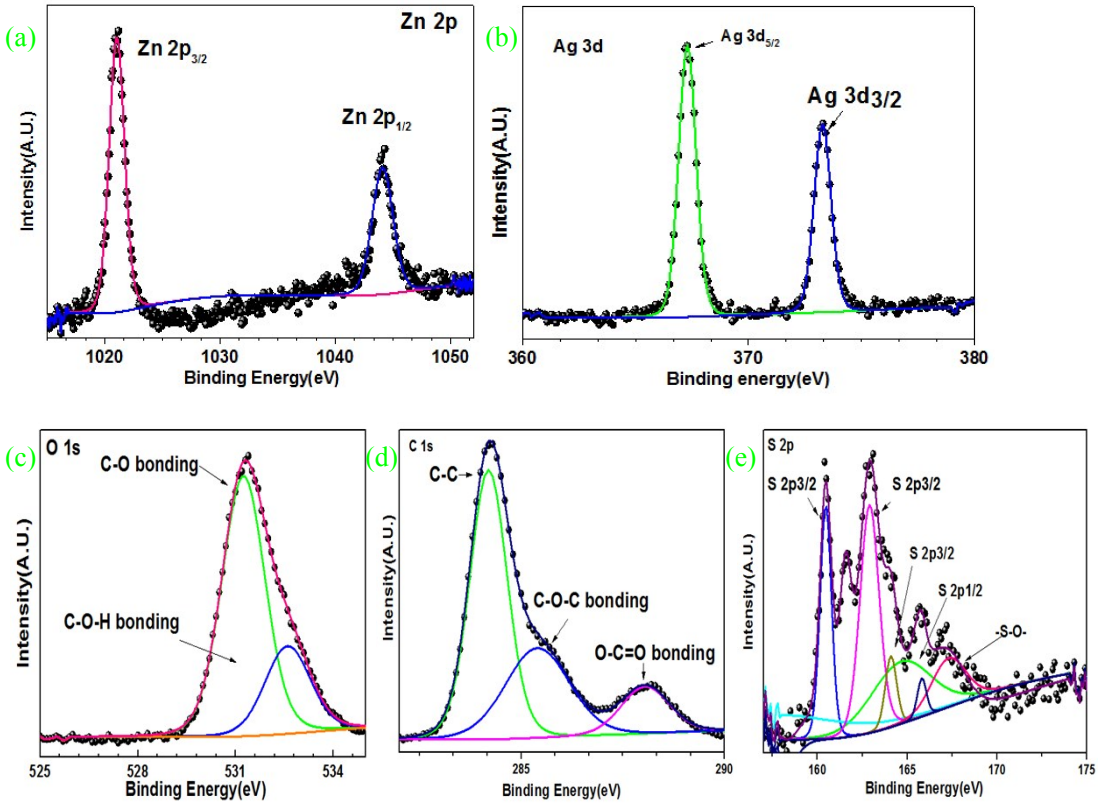

Figure S8. High resolution XPS spectra of Ag-Zn compound: (a) Zn 2p ; (b) Ag 3d; (c) S 2p; (d) C1s; (b) O 1s.

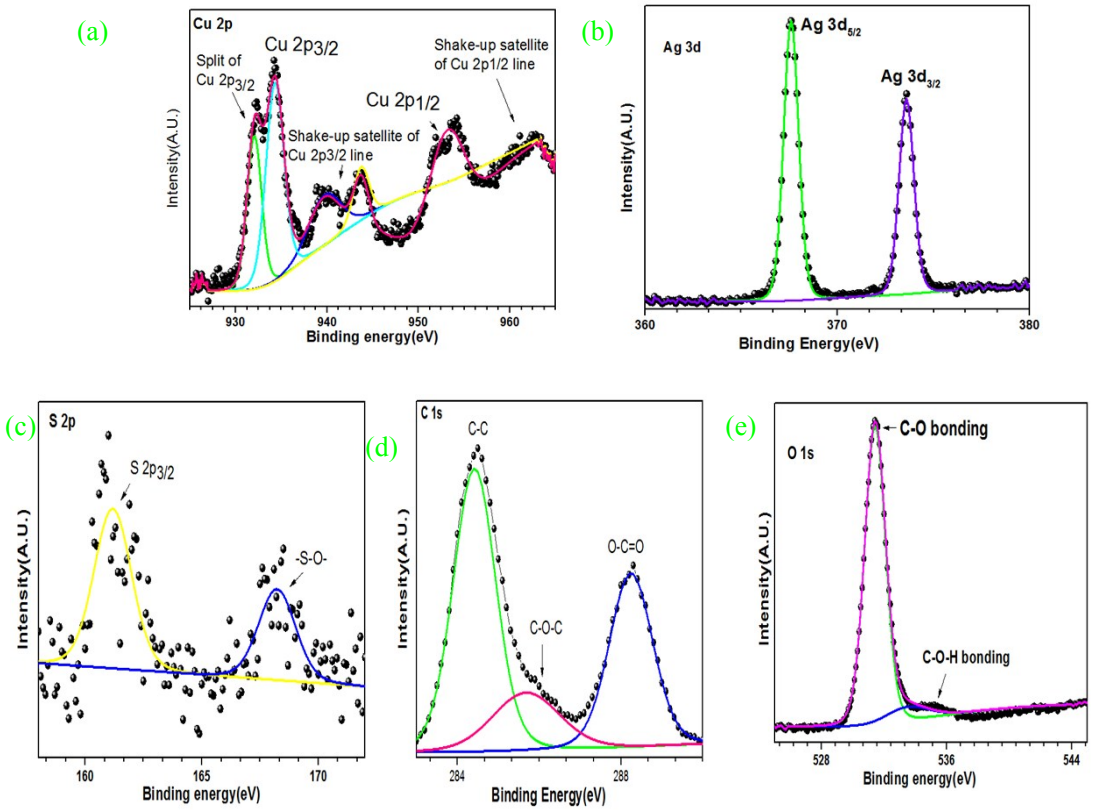

Figure S 9. High resolution XPS spectra of Ag-Cu compound: (a) Cu 2p; (b) Ag 3d; (c) S 2p; (d) C 1s; (e) O 1s.

For Ag-Cu compound(see Figure S9), the XPS spectra of Cu 2p show peaks at 932.0 eV, 934.3 eV, 939.9 eV, 943.7 eV, 953.5 eV and 961.1 eV. The peaks at 932.0 eV, 934.3 eV are due to the split of Cu $2p_{3/2}$. The peaks at 939.9 eV and 943.7 eV are considered as shake-up satellite of Cu 2p3/2 line. The peak at 953. 5 eV is attributed to Cu $2p_{1/2}$ core level. The peak at 961.1 eV is regarded as shake-up satellite of Cu $2p_{1/2}$ line. [s7] Ag 3d spectra show two peaks at 367.6 eV and 373.6 eV, which are assigned to which are assigned to core level of Ag $3d_{5/2}$ and Ag $3d_{3/2}$.[s2] S 2p spectra produce two peaks at 161.2 eV and 168. 2 eV, which are assigned to S-O bonding. [s3] C 1s spectra show peaks at 284.4 eV, 285.7 eV and 288.3 eV, which are considered as C-C bonding,.[s4] C-O-C bonding and O-C=O. [s4,s5] O1s spectra show peaks at 531.4 eV and 534.4 eV, which are attributed to C-O bonding and C-O-H bonding. [s4, s6]

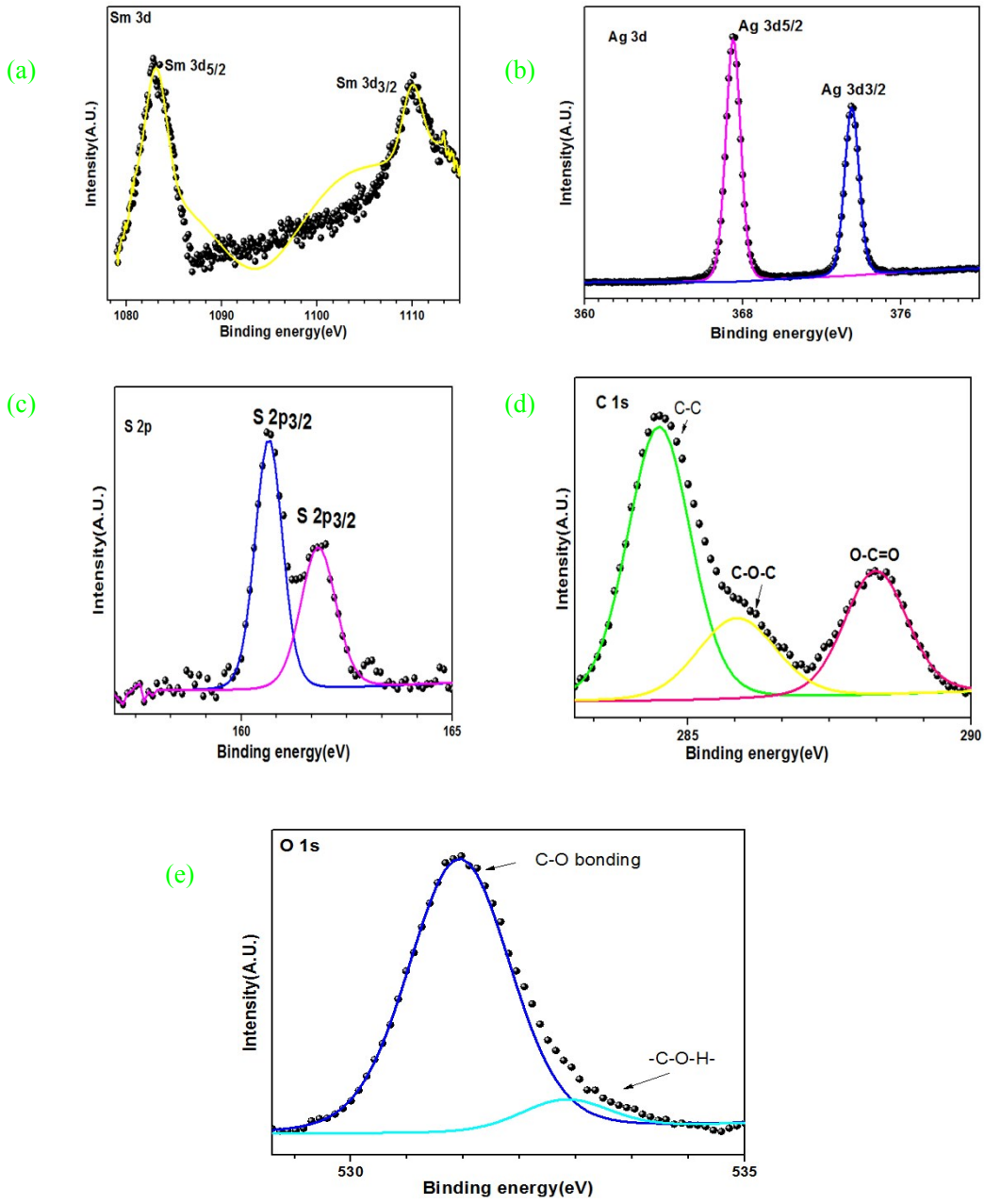

Figure S 10. High resolution XPS spectra of Ag-Sm compound: (a) Sm 3d; (b) Ag 3d;(c) S 2p; (d) C 1s; (e) O 1s.

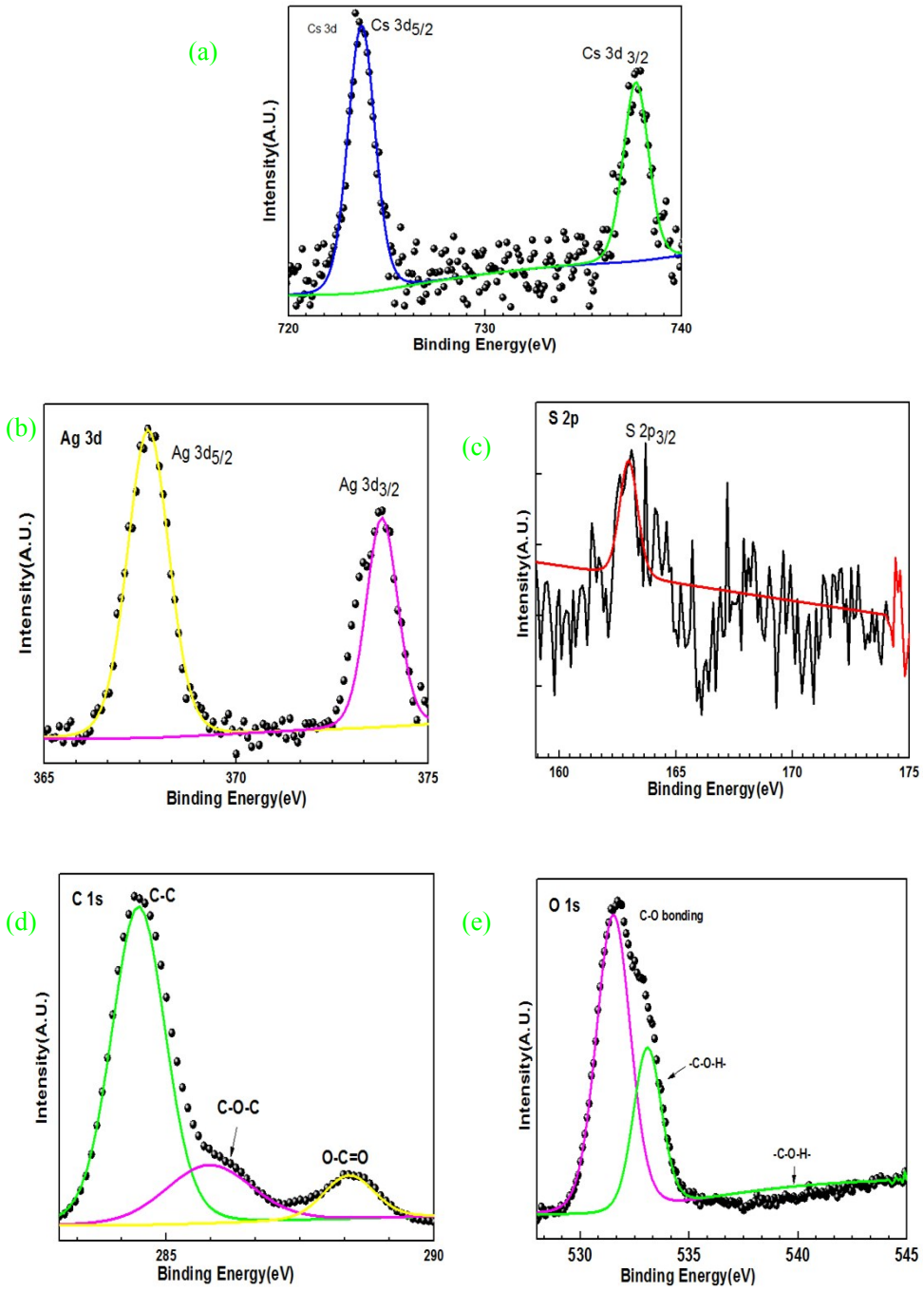

Figure S 11. XPS spectra of Ag-Cs compound: (a) Cs 3d; (b) Ag 3d; (c) S 2p; (d) C 1s; (e) O 1s.

For **Ag-Sm** compound(see Figure S10), the XPS spectra of Sm 3d show peaks at 1083 eV, 1110 eV, which are assigned to Sm $3d_{5/2}$, Sm $3d_{3/2}$.[s8] Ag 3d spectra present peaks at 367.5 eV and 373.6 eV, which are related with Ag $3d_{5/2}$, Ag $3d_{3/2}$. [s2] The high-resolution of S 2p XPS spectra show peaks at 160.7 eV and 161.8 eV, which are both assigned to S $2p_{3/2}$. [s3] C 1s spectra show peaks at 284.5 eV, 285.9 eV and 288.3 eV, which are considered as C-C bonding,[s4] C-O-C bonding [s4]and O-C=O.[s5] O1s spectra show peaks at 531.4 eV and 532.9 eV, which are attributed to C-O bonding and C-O-H bonding.[s4, s6]

For **Ag-Cs** compound (see Figure S11), the Ag 3d orbital shows XPS transitions for 3d5/2 and 3d3/2 at 367.7 eV and 373.8 eV, respectively.[s2] The high resolution XPS spectra of Cs 3d for Ag-Cs

compound show two distinctive peaks at 723.7 eV and 737.6 eV, respectively. The peak at 723.7 eV is corresponding to the CS $3d_{5/2}$.[s9] The peak at 737.6 eV is assigned to CS $3d_{3/2}$.[s10] These signals were likely due to the presence of Ag and Cs in the C-H-O-S matrix. Deconvolution of S 2p spectra shows a peak at 162.9 eV which can be assigned to S $2p_{3/2}$. [s3] C 1s XPS spectra show two peaks at 284.4 eV, 288.4 eV and a shoulder at 285.8 eV. They are assigned to C-C bonding, C-O-C bonding and O-C=O bonding, respectively.[s4,s5] Deconvolution of O 1s spectra produces two main peaks around 531.5 eV, 533 eV and a subpeak around 540 eV. The peak around 531.5 eV is assigned to C-O.[s4]The peak around 533 eV is attributed to C-H-O bonding.[s5] The peak around 540 eV is assigned to C-O-H bonding.[s6]

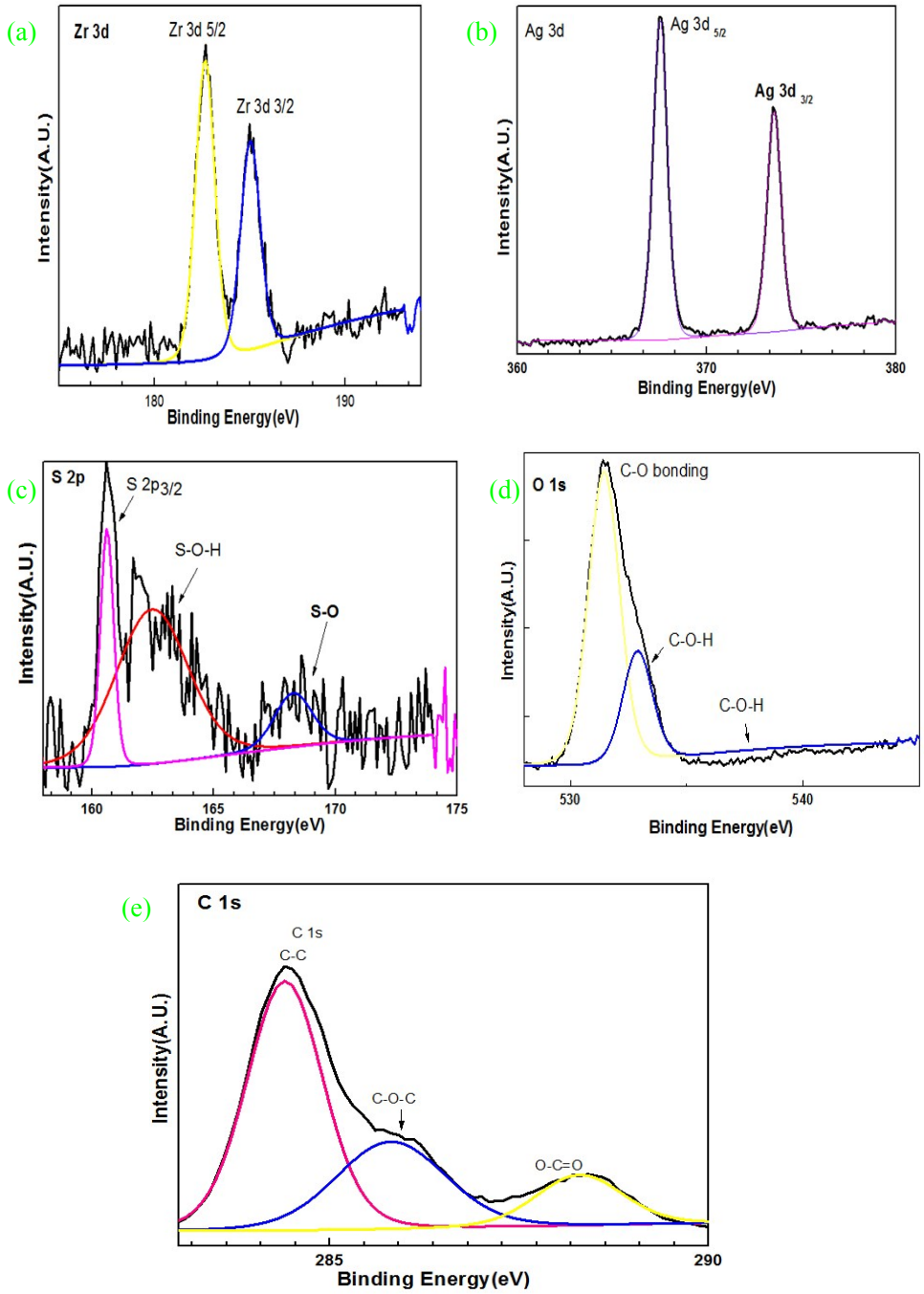

Figure S12. XPS spectra of Ag-Zr compound: (a) Zr 3d; (b) Ag 3d; (c) S 2p; (d) C 1s ; (e) O 1s.

The high resolution XPS spectra of Ag 3d for **Ag-Zr** compound present two distinctive peaks at 367.5 eV and 373.6 eV, respectively. They are corresponding to Ag $3d_{5/2}$ (367.5 eV) and Ag $3d_{3/2}$ (373.6 eV).[s2] The high resolution XPS spectra of Zr 3d for Ag-Zr compound present two distinctive peaks at 182.7 eV and 185.1 eV, respectively. They are corresponding to Zr 3d5/2 (182.7 eV) and Zr 3d3/2.[s11] The deconvolution of XPS spectra of S 2p presents 160.6 eV, 162.5 eV, 168.3 eV. The peak at 160.6 eV is assigned to S $2p_{3/2}$. [s12] The peak at 162.5 eV is assigned to S-H-O bonding, which may be generated from the compound of L-Cysteine in the reaction.[s12] The peak at 168.3 eV is assigned to S-O bonding, which may be related with sulfuric acid in the reaction. [s12] C 1s spectra present peaks at 284.4 eV, 285.9 eV and 288.3 eV, which are corresponding to C-C bonding, C-O-C bonding, O-C=O bonding. [s4,s5]

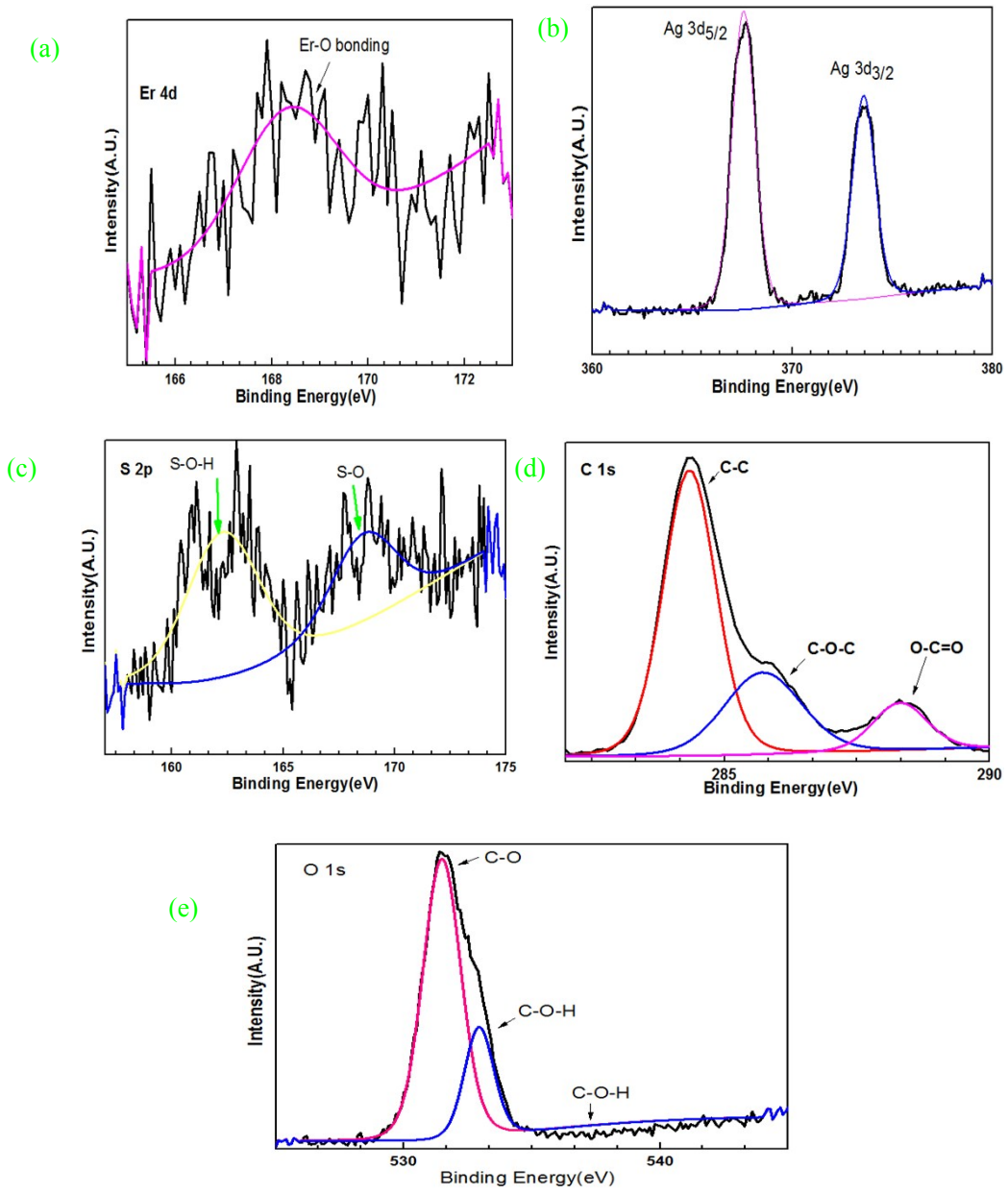

Figure S13. XPS spectra of Ag-Er compound : (a) Er 4d; (b) Ag 3d; (c) S 2p; (d) C 1s; (e) O 1s.

The high resolution XPS spactra of Er 4d for **Ag-Er** compound present a peak at 168.4 eV, which is comparable to Er-O bonding in Er_2O_3. [s14] The high resolution XPS spectra of Ag 3d for Ag-Er compound present two distinctive peaks at 367.6 eV and 373.6 eV, respectively. They are corresponding to Ag 3d5/2 (367.6 eV) and Ag 3d3/2 (373.6 eV).[s2] The XPS spectra of S 2p show peaks at 162.4 eV and 168.8 eV. The peak at 162.4 eV is attributed to S-O- H bonding.[s12] The peak at 168.8 eV is considered to be related with S-O bonding. [s12] C 1s spectra present peaks at 284.4 eV, 285.7 eV and 288.3 eV, which are assigned to the main peak of C 1s, C-O-C bonding, O-C=O bonding. [s4,s5] XPS spectra of O 1s show peaks at 531.5 eV, 532.9 eV and 539.3 eV, which are assigned to C-O bonding,[s4] C-O-H bonding,[s5]C-O-H bonding,[s6] respectively.

The high resolution XPS spectra of Ag 3d for **Ag-Y** compound present two distinctive peaks at 367.4 eV and 373.5 eV, respectively. They are corresponding to Ag $3d_{5/2}$ (367.4 eV) and Ag $3d_{3/2}$ (373.5 eV). [s2] XPS spectra of Y 3d show peaks at 152.8 eV, 157.8 eV, 160.2 eV and 163.1 eV. The peaks of 157.8 eV and 160.2 eV are assigned to Y $3d_{5/2}$ and Y $3d_{3/2}$, respectively. [s15] The other two peaks of 152.8 eV and 163.1 eV are possibly indexed as Y $3d_{7/2}$ and Y $3d_{1/2}$. XPS spectra of S 2p show peaks at 160.3 eV and 163.4 eV. The peak of 160.3 eV is attributed to the main peak of S $2p_{3/2}$. The peak at 163.4 eV is assigned to S-H-O bonding.[s12] C 1s spectra show peaks at 284.2 eV,285.6 eV, 288.3 eV, which are assigned to C-C bonding, C-O-C bonding, O-C=O bonding.[s4,s5] O 1s spectra present peaks at 531.6 eV and 533.1 eV, which are related with C-O bonding, C-O-H bonding. [s4,s5]

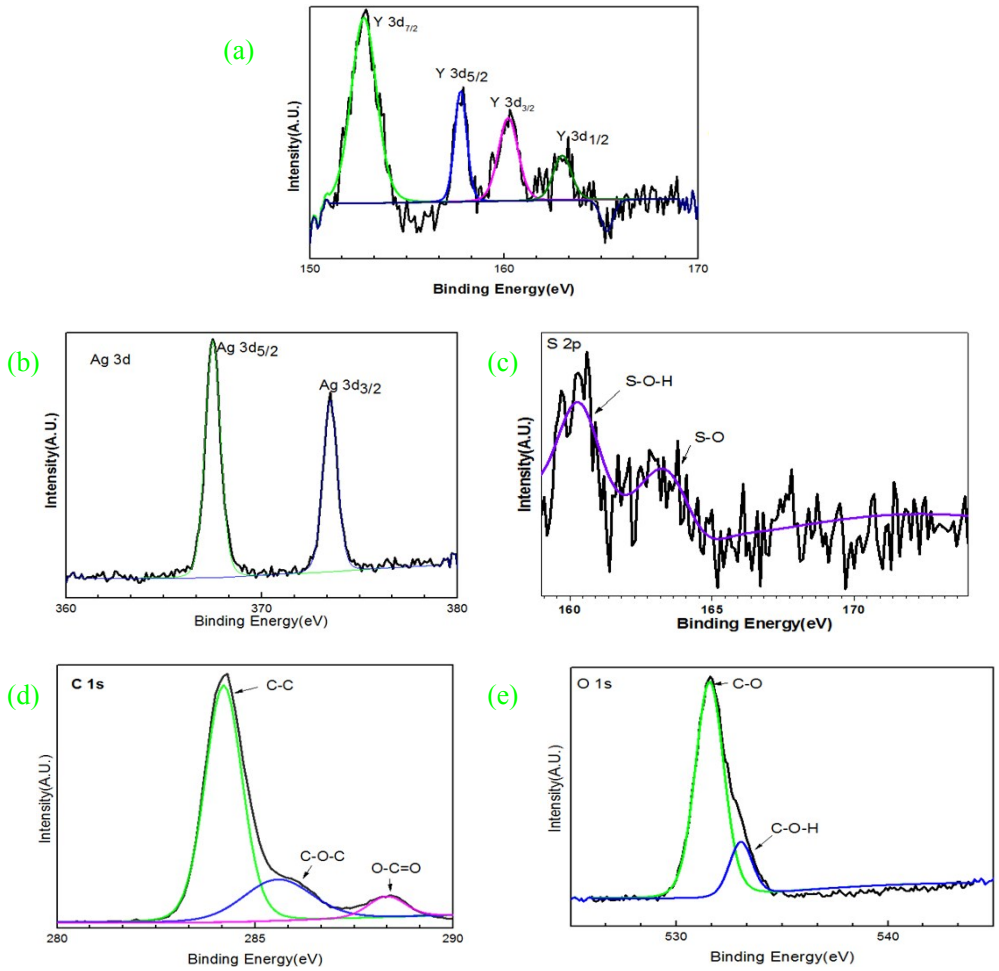

Figure S 14. XPS spectra of Ag-Y compound: (a) Y 3d; (b) Ag 3d; (c) S 2p; (d) C 1s; (e) O 1s.

For Ag-Co compound, XPS spectra of Ag 3d show peaks at 367.4 eV, 373.3 eV, which are indexed with Ag $3d_{5/2}$ and Ag $3d_{3/2}$.[S2] XPS spectra of Co 2p show peaks at 780.1 eV, 783.9 eV, 796.9 eV, 801.7 eV. The peak at 780.1 eV is main peak of Co $2p_{3/2}$. The peak at 783.9 ev is satellite peak of Co $2p_{3/2}$. The peak at 796.9 eV is satellite peak of Co $2p_{1/2}$. The peak at 801.7 eV is main peak of Co $2p_{1/2}$.[S17] XPS spectra of S 2p show peaks at 160.6 eV, 162.3 eV and 163.1eV, which are indexed with S 2p3/2, S-C-N-O-H bonding and S-C-O-H bonding.[S12] C 1s spectra present peaks at 284.4 eV,285.6 eV, 288.1 eV, which are assigned to C-C bonding, C-O-C bonding, O-C=O bonding. [S4] XPS spectra of O 1s show peaks at 531.2 eV, 532.7 eV, which are assigned to C-O bonding and C-O-H bonding.[S4,S5]

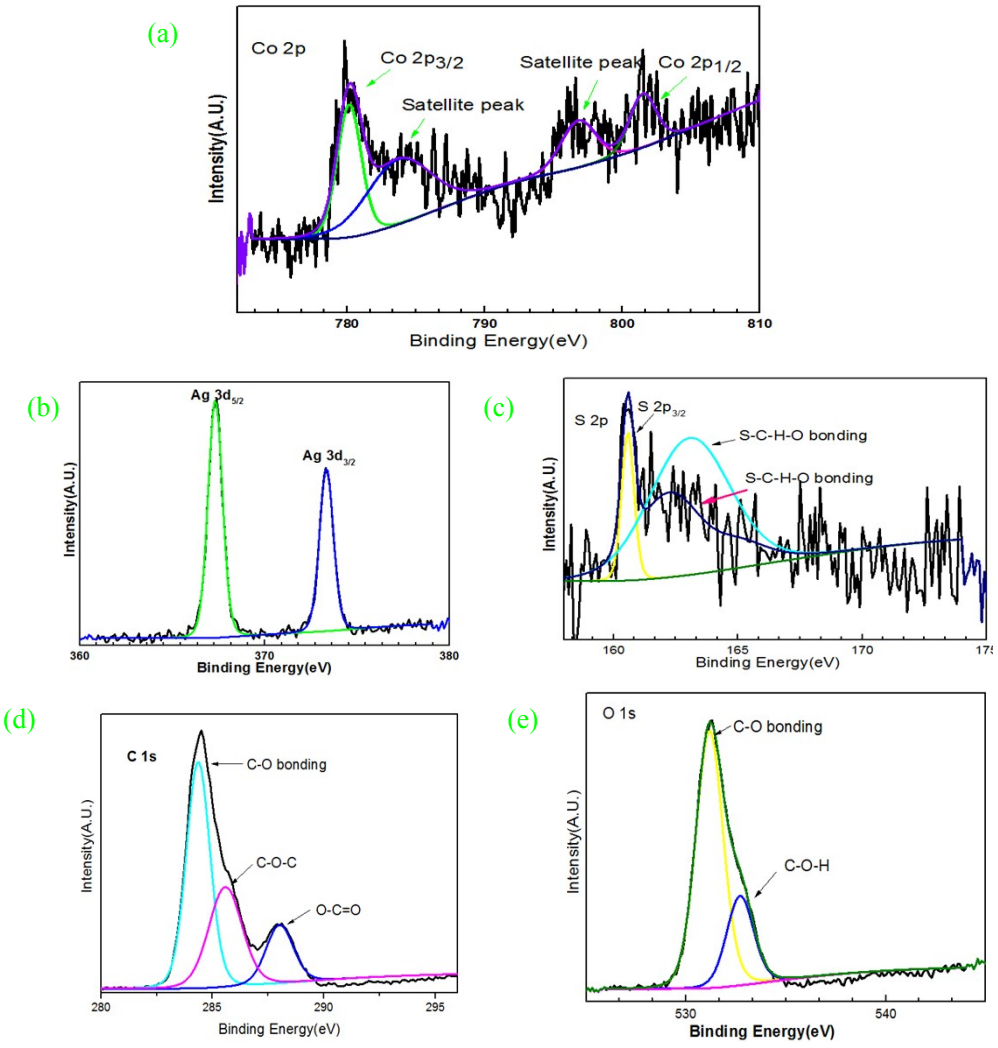

Figure S 15. XPS of Ag-Co compound : (a) Co 2p; (b) Ag 3d; (c) S 2p; (d) C 1s; (e) O 1s.

References:

(s1) Bhunia, S.; Molla, R. A.; Kumari, V. ; Islam, Sk. M. ; Asim Bhaumik. Zn(II) assisted synthesis of porous salen as an efficient heterogeneous scaffold for capture and conversion of CO_2. *Chem. Commun.*, **2015**, 51, 15732.

(s2) Tjeng, L. H.; Meinders, M. B. J.; Elp, J. van; Ghijsen, J.; Sawatzky, G. A. Electronic structure of Ag_20. Phys. Rev. B 1990, 41, 3190-3199.

(s3) Smart, R. St. C.; Skinner,W. M.; Gerson, A. R. XPS of Sulphide Mineral Surfaces:Metal-deficient, Polysulphides, Defects and Elemental Sulphur. Surf. Interface Anal. 1999, 28, 101-105.

(s4) (a) Dubal, D. P.; Chodankar, N. R.; Caban-Huertas, Z.; Wolfart,F.; Vidotti, M.; Holze, R.; Lokhande, C. D.; Gomez-Romero, P. Synthetic approach from polypyrrole nanotubes to nitrogen doped pyrolyzed carbon nanotubes for asymmetric supercapacitors. J. Power Sources 2016, 308, 158e165. (b) Sheng, Z. -H., Shao, L. , Chen,J. -J.; Bao, W. -J. ; Wang,F. -B. ; Xia, X. -H. Catalyst-Free Synthesis of NitrogenDoped Graphene via Thermal Annealing Graphite Oxide with Melamine and Its Excellent Electrocatalysis. ACS Nano, 2011, 5, 4350-4358.

(s5) Ganguly, A.; Sharma,S.; Papakonstantinou, P.; Hamilton, J. Probing the Thermal Deoxygenation of Graphene Oxide Using High-Resolution In Situ X-ray-Based Spectroscopies. J. Phys. Chem. C 2011, 115, 17009-17019.

(s6) Desimoni, E.; Casella,G. I.; Morone, A.; Salvi, A. M. XPS Determination of Oxygen-containing Functional Groups on Carbon-fibre Surfaces and the Cleaning of These Surfaces. Surf. Interf. Anal. 1990, 15,627434.

(s7) Skinner, W. M. ; Prestidge, C. A. ; Smart, R. St. C. Irradiation Effects During XPS Studies of Cu(II) Activation of Zinc Sulphide. Surf. Interf. Anal. 1996, 24, 620-626.

(s8) Suga, S.; Imada, S. ; Ochiai, A.; Suzuki, T. XPS and BIS studies of electronic structures of Sm3Se 4 and Sm4As3. Physica B 1993, 186,59-62

(s9) Berghe, S. Van den; Laval, J. -P.; Gaudreau, B.; Terryn, H.; Verwerft, M. XPS investigations on cesium uranates: mixed valency behaviour of uranium. J. Nuclear Mat. 2000,277,28-36.

(s10) Zaman,S. F.; Pasupulety, N.; Al-Zahrani, A. A.; Daous, M. A.; Driss, H.; Al-Shahrani, S. S.; Petrov, L. Influence of alkali metal (Li and Cs) addition to Mo_2N catalyst for CO hydrogenation to hydrocarbons and oxygenates. The Can. J. Chem. Eng. 2018, 96, 1770-1779.

(s11) Tsunekawa,S.; Asami, K.; Ito, S. ; Yashima, M.; Sugimoto, T. XPS study of the phase transition in pure zirconium oxide nanocrystallites. Appl. Surf. Sci. 2005, 252, 1651-1656.

(s12) Kelemen, S. R.; George, G. N.; Gorbaty, M. L. Direct determination and quantification of sulphur forms in heavy petroleum and coals 1. The X-ray photoelectron spectroscopy (XPS) approach. Fuel, 1990, 69, 939-944.

(s13) Dubal, D. P.; Chodankar, N. R.; Caban-Huertas, Z.; Wolfart, F.; Vidotti, M.; Holze, R.; Lokhande, C. D.; Gomez-Romero, P. Synthetic approach from polypyrrole nanotubes to nitrogen doped pyrolyzed carbon nanotubes for asymmetric supercapacitors. J. Power Sources, 2016, 308 158-308165.

(s14) Speranza, G.; Calliari, L.; Ferrari, M.; Chiasera, A.; Ngoc, K. T.; Baranov, A. M.; Sleptsov, V. V.; Nefedov, A. A.; Varfolomeev, A. E.; Fanchenko, S. S. Erbium-doped thin amorphous carbon films prepared by mixed CVD sputtering. Appl. Surf. Sci. 2004, 238, 117-120.

(s15) Jafer, R. M.; Coetsee, E.; Yousif, A.; Kroon, R. E.; Ntwaeaborwa, O. M.; Swart, H. C. X-ray photoelectron spectroscopy and luminescent properties of $Y_2O_3:Bi^{3+}$ phosphor. Appl. Surf. Sci. 2015, 332, 198-204.

(s16)Pashutski, A.; Folman, M. Low temperature XPS studies of NO and NO2 Adsorption on Al (100). Surf. Sci. 1989, 216, 395-408.
(s17) Tan, B. J.; Klabunde, K. J.; Sherwood, P. M. A. XPS studies of solvated metal atom dispersed (SMAD) catalysts. Evidence for layered cobalt-manganese particles on alumina and silica. J. Am. Chem. Soc., 1991, 113, 855-861.